Available online at BCREC website: https://bcrec.id

Bulletin of Chemical Reaction Engineering & Catalysis, 17 (4) 2022, 786-797

Research Article

Preparation of B/ZnO Nanocomposite by Simple Mechanical Combustion Method for Removal of Antibiotics in Aqueous Environments

Thu Huong Nguyen, Anh - Tuan Vu*

School of Chemical Engineering, Hanoi University of Science and Technology, Hanoi, Vietnam.

Received: 6th October 2022; Revised: 22nd November 2022; Accepted: 22nd November 2022
Available online: 7th December 2022; Published regularly: December 2022

Abstract

In this study, the B/ZnO nanocomposite was successfully synthesized by a simple mechanical combustion method. This material was used as a photocatalyst to degrade tetracycline, a representative of the commonly used antibiotics today. The B/ZnO composite became tighter than that of pure ZnO and formed bulk particles. The band gap energy of B/ZnO (3.05 eV) was slightly lower than that of ZnO (3.10 eV), resulting that it being easier to absorb visible light to create electron-hole pairs (h^+ and e^-). Therefore, the B/ZnO composite had higher photocatalytic activity than pure ZnO. The ratio of boron-doped to ZnO affecting the photocatalysis efficiency was investigated and the optimal boron content was 3 wt%, its degradation efficiency (DE) value for tetracycline hydrochloride (TCH) in 90 min and the rate constants were 90% and 0.054 min^{-1}, respectively. The factors affecting the photocatalytic process like initial antibiotic concentration, catalyst content, and pH of the initial antibiotic solution were studied. In addition, the recovery and reuse of B/ZnO after photocatalytic treatment were also studied.

Keywords: ZnO; B/ZnO; Photocatalyst; Antibiotics; Visible Light

How to Cite: T.H. Nguyen, A.T. Vu (2022). Preparation of B/ZnO Nanocomposite by Simple Mechanical Combustion Method for Removal of Antibiotics in Aqueous Environments. *Bulletin of Chemical Reaction Engineering & Catalysis*, 17(4), 786-797 (doi: 10.9767/bcrec.17.4.16090.786-797)

Permalink/DOI: https://doi.org/10.9767/bcrec.17.4.16090.786-797

1. Introduction

Environmental pollution is always a hot topic in society, especially water pollution is becoming more serious. In recent years, antibiotic contamination has been recognized as water pollution because of its potential adverse effects on ecosystems and human health [1–4]. Most antibiotics used for humans and animals are excreted into the environment as intact or decomposed from variety of pathways, including hospital wastewater, domestic wastewater, and pharmaceutical factory wastewater. In addition, antibiotics are also widely used in animal, that leads the untreated manure and animal feed status being discharged directly into the environment causing the antibiotic pollution [2]. Notably, in surface water and groundwater domestic water more than dozens of antibiotics sulfonamide, tetracycline and fluoroquinolone were detected [5]. Tetracycline is a broad-spectrum antibiotic widely used in humans and animals, which is active against a number of gram-negative and gram-positive bacteria. However, widespread use and release of antibiotics into the environment could lead to bacterial resistance to antibiotics and cause severe problems in humans [1–5]. Therefore, it requires methods to remove antibiotic residues in the aquatic environment.

At present, there are many methods to treat excess antibiotics, such as physical adsorption,

* Corresponding Author.
Email: tuan.vuanh@hust.edu.vn (A.T. Vu);
Telp: +84-912911902, Fax: +84-02438680070

biodegradation, advanced oxidation, coagulation, electrolysis [1,5]. In which, the oxidation of organic compounds method by air oxygen using nanomaterials as photocatalysts under the influence of sunlight has been widely researched and developed [5–8]. Although ZnO has a large band gap energy (~3.37 eV), exhibiting high electric breakdown field and thermal conductivity, it attracts much attention from researchers due to its easy synthesis, low cost, nontoxicity, and reusability. In the photocatalysis process, the band gap energy of the catalyst is an important factor. When a photocatalyst absorbs light radiation with an energy greater than its band gap energy, electrons move from the valence band (VB) to the conduction band (CB), photodegradation reaction occurs on its active surface through the formation of $OH^{\bullet}$ and $O_2^{\bullet -}$, which rapidly breakdown target pollutants into the end products of CO_2 and H_2O [9]. Therefore, the small band gap energy can facilitate the light absorption capacity of the catalyst, which improves the photocatalyst efficiency.

Under the radiation of light, the electrons and holes created by ZnO can decompose organic substances. However, there are also some limitations when using ZnO as a photocatalyst, such as low sunlight absorption due to high band gap energy, and the electron-hole recombination process taking place rapidly emerging, that has limited its practical applications [10]. To improve the photocatalytic performance of ZnO, it is common to dope an appropriate amount of metals, such as gold (Au) [6,11–14], silver (Ag) [15–17], and tin (Sn) [18,19], or nonmetals, such as boron (B) [18,20], nitrogen (N) [21], *etc*., to enhance the ability to absorb sunlight, prevent electron recombination and holes, improve the particle size, increase the surface area, and improve the photocatalytic degradation of organic substances [18–25]. Among them, B doping has attracted great interest due to its atomic size and electronic structure [18,20]. Currently, there are many different methods have been used to synthesize B/ZnO nanomaterials such as the sol-gel method, and the combustion method. In 2020, Raisa Estefanía Núñez-Salas and colleagues studied preparation of B/ZnO by sol-gel method on photocatalytic inactivation of *Escherichia coli* and *Enterococcus sp* [20]. This method can synthesize fine, nano-sized materials. Abrar Zadeed Ahmed and colleagues studied the fabrication and characterization of B/Sn-doped ZnO nanoparticles via the mechanochemical method for photocatalytic degradation of rhodamine B [18]. This method can simply synthesize materials in a short time. However, there are still some limitations including unequal size materials, heterogeneous morphology, and low performance.

In this study, B/ZnO was synthesized by a simple mechanical combustion method and then characterized by UV-Vis/DR, XRD, SEM, and FT-IR methods. The photocatalytic degradation efficiency of B/ZnO was investigated by reaction with tetracycline hydrochloride. The factors affecting the photocatalytic ability of materials such as initial antibiotic concentration, catalyst content, and pH of the initial antibiotic solution were studied. In addition, the recovery and reuse of B/ZnO materials were also studied. The first-order kinematics graph was used for the calculations.

2. Materials and Methods

2.1 Materials

Zinc acetate dehydrates ($Zn(CH_3COO)_2.2H_2O$, 99%), oxalic acid dehydrates ($C_2H_2O_4.2H_2O$, 99.5%) and boric acid (H_3BO_3, 99.8%) were purchased Xiong Scientific Co., Ltd, China. Tetracycline hydrochloride ($C_{22}H_{24}N_2O_8.HCl$, 99%) was purchased from Hefei BoMei Biotechnology Co., Ltd, China. All chemicals were used without any purification and distilled water was used during the evaluation of the photocatalytic potential of the materials.

2.2 Methods

Ultraviolet-visible diffuse reflectance (UV–Vis/DR) spectroscopy was used to investigate the light absorption capacity and determine the band gap energy of the material samples. The samples were characterized by powder X-ray diffraction (XRD) using a Bruker D8 Advance diffractometer (Germany) with Cu K_α radiation (λ = 1.54060). The morphology of the samples was observed using a scanning electron microscope (SEM JEOL series 7600F). Fourier infrared spectroscopy (FTIR, Madison, WI, USA) was performed to determine the Zn−O, B−O, and O−H bonds (in Zn−O−H and H−O−H) in the research sample.

2.3 The Preparation of Materials

The synthesis process of ZnO and B/ZnO was carried out according to the previous paper with some modifications [18]. ZnO and B/ZnO nanoparticles were synthesized by simple mechanical combustion (Figure 1). In the synthesis, initially, 2.195 g zinc acetate dihydrate and 2.521 g oxalic acid dihydrate were mixed and

ground in an agate mortar for 10 min to obtain a viscous mixture of zinc oxalate dehydrate and acetic acid (with a strong odor show). Then, boric acid (source also B) was added to the above mixture and the grinding process was continued for another 10 min to obtain the precursor. Finally, the precursor was calcined in air at 500 ℃ for 3 h with a heating rate of 10 ℃/min, then ZnO and B/ZnO were obtained. To investigate the effect of the content of B doping on ZnO on the photocatalytic efficiency, the mass of boric acid was taken so that %wt B doping on ZnO was 1, 3, 5, and 7, and the samples were named B/ZnO–1, B/ZnO–3, B/ZnO–5 and B/ZnO–7, respectively.

2.4 Photocatalysis Procedure

The photocatalytic activity of the material samples was evaluated by degrading tetracycline hydrochloride (TCH). The experimental procedure is as follows: 0.05 g of catalyst was placed in a 250 mL beaker containing 100 mL of TCH solution of known concentration and sonicated for about 5 min to disperse the material evenly. The reaction beaker was stirred continuously at an average speed of 250 rpm and placed in the dark to achieve the desired state of adsorption/desorption. Then, the reaction cup was irradiated with a 250 W Hg lamp. After each specified time interval, 3 mL of the suspension was filtered through a Millipore filter (0.45 μm PTFE membrane) and the residual TCH concentration was measured using a UV-Vis spectrometer (Agilent 8453) at a maximum wavelength of 375 nm. The degradation efficiency (DE), the rate constant, and degradation capacity (DC) of the TCH are calculated according to Equations (1), (2), and (3), respectively [9,26]:

$$DE = \frac{C - C_0}{C_0} \times 100 \quad (1)$$

$$\ln\left(\frac{C_0}{C}\right) = kt \quad (2)$$

$$DC = \frac{(C_0 - C_t) \times V}{m} \quad (3)$$

where, C is the solution concentration at time t; C_0 is the initial solution concentration; k is the degradation rate constant; t is the time; V is the solution volume; m is the mass of catalyst.

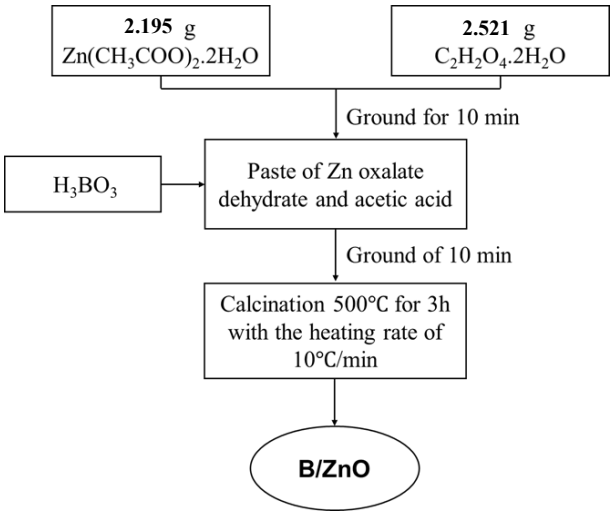

Figure 1. Synthesis of B/ZnO nanoparticles by mechanochemical combustion method.

3. Results and Discussion

3.1 The Optimal Boron Content Survey

Figure 2 shows the UV-Vis/DR spectrum and the graph of band gap determination of the

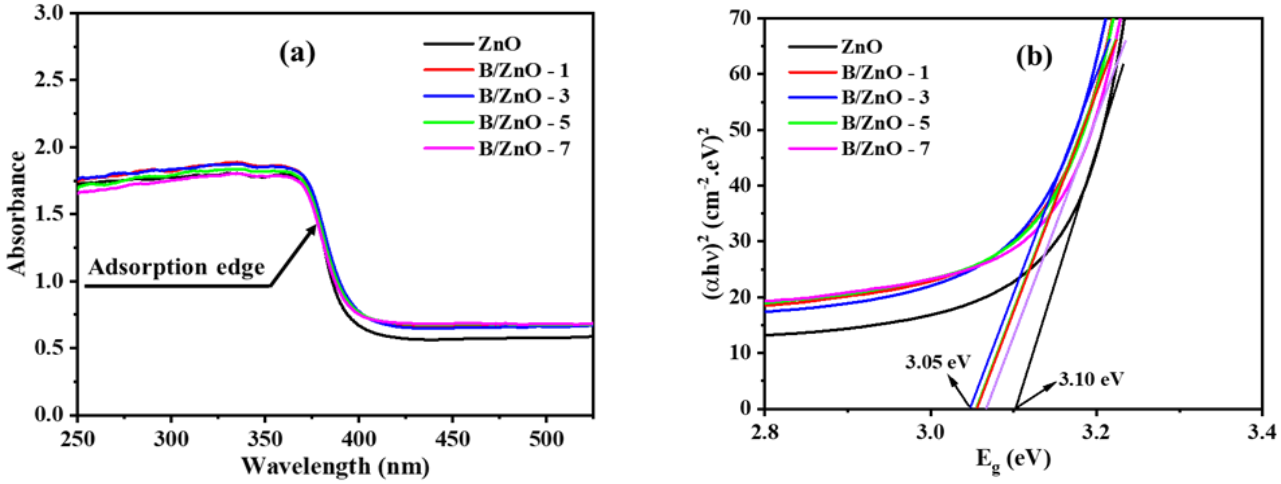

Figure 2. (a) The DR/UV–Vis spectra and (b) Tauc plot of samples ZnO and B/ZnO–1, B/ZnO–3, B/ZnO–5, B/ZnO–7.

samples ZnO, B/ZnO–1, B/ZnO–3, B/ZnO–5, and B/ZnO–7. Through Figure 2(a), it was found that the dispersion of B particles on ZnO increased the absorption of B/ZnO material compared with pure ZnO, especially the curve showing the absorption of B/ZnO–3 has the highest increase compared to the remaining samples. All samples have strong absorption in the UV region. From the graph of the relationship between ($h\nu$) and $(\alpha h\nu)^2$, it is possible to calculate the band gap energies of the samples through the Tauc method [25] according to the equation:

$$(\alpha h\nu)^{1/n} = A(h\nu - E_g) \quad (4)$$

where, E_g is the band gap energy; α is the absorption coefficient of the material; h is the Plank's constant; ν is the frequency of light; A is a constant; n is determined by the optical transition type of the semiconductor.

Here, ZnO exhibits a direct optical transition so the value n = 1/2. As shown in Figure 2(b), the band gap energy value of the ZnO sample is 3.10 eV, which was 3.06 eV for both samples B/ZnO–1 and B/ZnO–5, and 3.07 eV for B/ZnO–7. Meanwhile, the band gap energy of B/ZnO–3 is 3.05 eV, the lowest of all samples. Therefore, the optimal doped boron content was 3 wt%.

In addition, Figure 3 shows the degradation of TCH with ZnO and B/ZnO catalysts with different B-doped content on ZnO under the same conditions: antibiotic concentration [TCH] = 20 mg/L, catalyst content = 0.5 g/L, the light source was 250W Hg lamp. Because the TCH concentration was small, below 30 mg/L, and the degradation mechanism of TCH in the catalyst followed the generation of free radicals, the photocatalytic degradation rate of TCH can be studied using the first-order kinetic model, which was expressed as Equation (2) (in section 2.4). The graph in Figure 3(b) shows plots of ln (C_0/C) versus time. The slope value was used to determine the degradation rate constant (k). R^2 values for all the B/ZnO samples were near 1. This shows that the first-order kinetics model is in good relation to the photodegradation process and can be employed to study the kinetics. This is completely consistent with the studies on the photocatalytic decomposition of organic matters [6,11–14]. The first-order rate constants determined for 0, 1, 3, 5 and 7% mass of boron on ZnO were 0.021, 0.048, 0.054, 0.046 and 0.030 min^{-1}, respectively. We see that, in 90 min, the TCH decomposition efficiency was 90% and the first order rate constant (k = 0.054 min^{-1}) was the highest. Thereby, the B/ZnO–3 sample can be concluded as the most effective photocatalyst to degrade TCH among as-prepared samples.

Combining the above factors, it can be concluded that the optimal content of doped boron

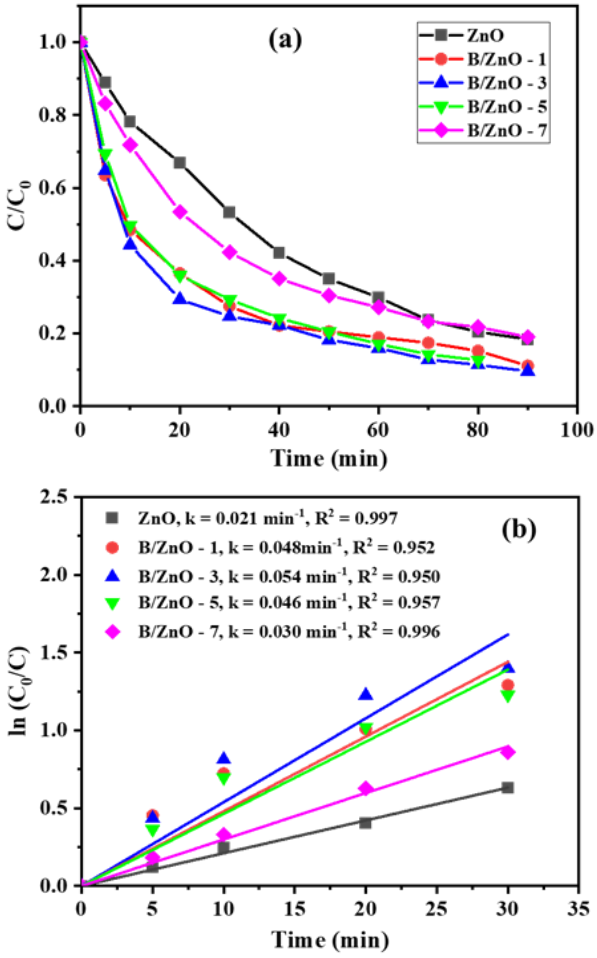

Figure 3. (a) The TCH decomposition ability of the catalyst with different concentrations of boron doped on ZnO; (b) kinematic curves.

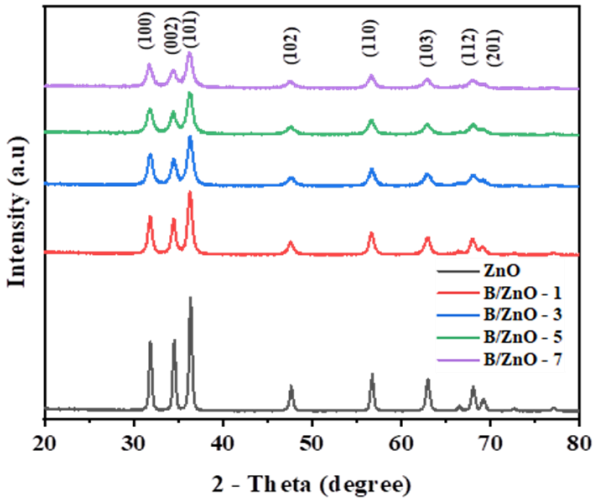

Figure 4. The XRD spectrum of ZnO and B/ZnO samples.

on ZnO was 3 wt%. Therefore, the B/ZnO–3 sample was used to analyze the structural and morphological characteristics through SEM, XRD, and FT-IR analysis to compare with ZnO. Also, the B/ZnO–3 sample was used to study the factors affecting the ability of photocatalysts to degrade antibiotics in water treatment.

3.2 Characterization of Prepared Photocatalysts

3.2.1 Structure properties

The XRD diffraction images of the synthesized ZnO and B/ZnO samples are shown in Figure 4. Comparing the XRD spectrum of pure ZnO and B/ZnO samples, no obvious difference was found. Besides, no impurity peaks were observed on all the synthesized material samples, thereby showing that the synthesized catalyst materials had high purity. All samples had lattice planes (100), (002), (101), (102), (110), (103), (112), and (201) corresponding to 2θ = diffraction peaks of 31.87; 34.57; 36.37; 47.65; 56.77; 63.00; 68.14; and 69.28° can be assigned to the hexagonal wurtzite structure of ZnO (JCPDS data: 036-1451) [27]. Thus, boron doping did not change the ZnO crystal structure. All the B/ZnO samples showed that the peak (101) was the strongest and the intensity of the peaks was decreased as the boron content increased. However, in the XRD spectrum of B/ZnO, no boron-related peaks were found. This could be explained by the low boron content and low crystallinity. The related peaks being covered by the peaks of ZnO and nanoparticles boron was very small.

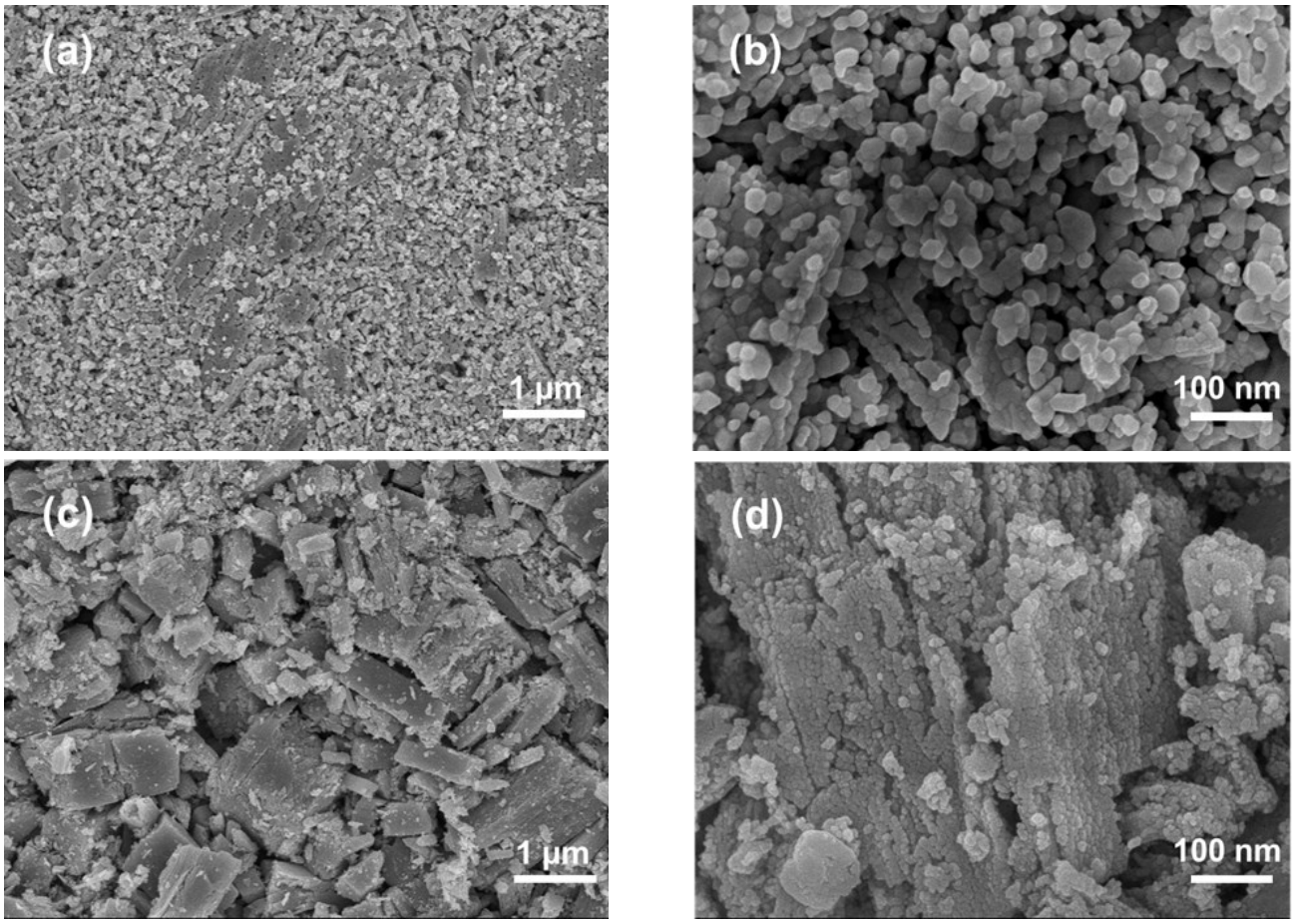

Figure 5. The SEM images of (a–b) ZnO, and (c–d) B/ZnO with different resolutions.

Table 1. The crystal sizes at different planes and average sizes of ZnO and B/ZnO samples.

		100	002	101	102	110	103	112	201	D (nm)
Crystallite size D (nm)	ZnO	19.5	19.4	18.3	15.7	15.9	13.3	13.0	12.5	16.0
	B/ZnO-1	12.2	11.6	11.2	9.5	10.5	9.0	8.8	9.3	10.2
	B/ZnO-3	9.5	7.9	9.0	7.6	8.3	7.2	6.3	8.7	8.1
	B/ZnO-5	8.2	7.1	8.5	8.0	7.9	6.9	6.5	8.8	7.7
	B/ZnO-7	8.0	6.6	8.4	7.5	8.2	7.1	6.3	9.0	7.6

We calculated the size of the ZnO and B/ZnO nanoparticles based on the Scherrer equation [18]:

$$D = \frac{K\lambda}{\beta \cos\theta} \quad (5)$$

where, K is a constant that depends on the crystal shape (usually K = 0.9); λ is the X-ray wavelength (1.5406 Å); θ is the Bragg diffraction angle; β is the line width of the sample corresponding to half the maximum intensity in radians (FWHM).

As the results are shown in Table 1, the average crystal size of ZnO nanoparticles was 16.0 nm and B/ZnO samples for 1, 3, 5, and 7 wt% of B were 10.2, 8.1, 7.7, and 7.6 nm, respectively. We see that the crystal size was decreased with increasing boron content. This size reduction might be due to the deformation in the crystal lattice of ZnO in the presence of boron in composites [18].

3.2.2 Morphological properties

Figure 5 shows the SEM images of ZnO and B/ZnO materials with different magnifications. Through the SEM image, it could be seen that the size and shape of the ZnO material changed when more boron was doped on the surface. The ZnO sample was observed to have heterogeneous morphology and unequal size as shown in Figure 5(a). As shown in Figure 5(b), it can be seen that ZnO was formed from zinc oxide nanoparticles of about 30–80 nm in size, which were closely arranged with each other. It can be seen from Figure 5(c) that as boron doping increased, the structure became tighter and formed bulks. Furthermore, the size of ZnO particles also became smaller with the size of about 30–50 nm (Figure 5(d)).

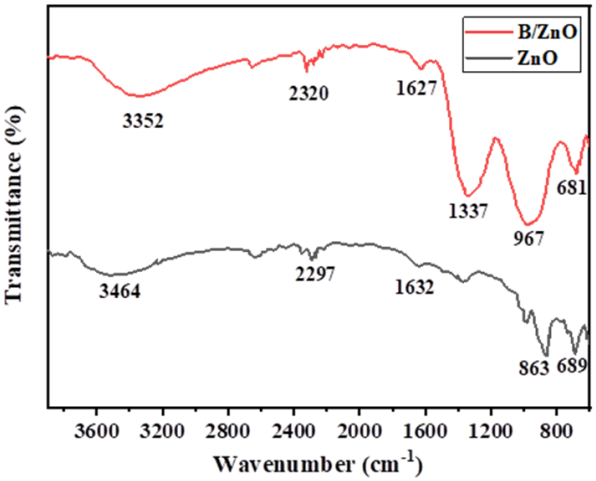

Figure 6. The FT-IR spectra of ZnO and B/ZnO samples.

The efficiency of the photodegradation reaction highly depended on the morphology, size, aggregation, and band gap energy of the photocatalyst [18]. The above research results show that although B/ZnO had a bulk shape and its structure was tighter than ZnO, its crystal size and band gap energy were smaller than ZnO. It was the expected morphology to increase the photocatalytic activity of the B/ZnO composite, which was presented in Section 3.1.

3.2.3 Fourier transform infrared spectroscopy

The FT-IR spectra of the ZnO and B/ZnO samples are shown in Figure 6. The bands at 3352, 1627 cm^{-1} and 3464, 1632 cm^{-1} corresponding to the IR spectra of covalent activity of O–H in adsorbed water (H–O–H) on B/ZnO and ZnO, respectively [18]. The relatively weak bands at 2297 and 2320 cm^{-1} were attributed to possible oscillations of C–H valence bond in environmental conditions [18]. The corresponding strong band at 1337 cm^{-1} on the IR spectrum of B/ZnO was attributed to the valence vibration of the B–O bond, indicating the association of boron with ZnO [18]. The small bands at 863 and 689 cm^{-1} of ZnO and 967 and 681 cm^{-1} of B/ZnO were thought to arise from the oscillations of the O–H bond in ZnO–O–H, respectively [28].

3.3 Investigation of Factors Affecting the Photocatalysis Process

3.3.1 Initial antibiotic concentration

In the study of materials, the effect of the initial antibiotic solution concentration on the photocatalytic efficiency is an important part. The initial concentration of TCH antibiotic solution was investigated in the range of 10-30 mg/L under the same reaction conditions as the catalyst content of 0.5 g/L, the light source was a 250W Hg lamp, and the results are shown in Figure 7. We see that an increase in the concentration of TCH caused a decrease in the decomposition efficiency. At initial concentration of 10 mg/L, TCH was completely decomposed in about 30 minutes. Meanwhile, after 90 minutes, B/ZnO achieved a degradation efficiency of 82% with the TCH concentration of 30 mg/L. The first-order rate constants of the TCH degradation reaction with initial concentrations of 10, 15, 20, 25, and 30 mg/L in the presence of photocatalyst B/ZnO were 0.126, 0.115, 0.054, 0.042, and 0.036 min^{-1}, respectively. This result could be explained by the following reasons: the formation of $\cdot OH^-$ and $\cdot O^{2-}$ on the surface of the catalyst and the probability

of •OH^- reacting with the antibiotic molecule. As the concentration of TCH increases, the photons are intercepted before they can reach the catalyst surface, and the generation of •OH^- and •O^{2-} radicals decrease, meaning that the decomposition efficiency of the TCH solution decreases. In addition, a large number of adsorbent antibiotics can compete for a constant total number of active sites available for adsorption at fixed catalyst concentrations [28]. However, when the concentration of TCH solution increases, the decomposition capacity also tends to increase. As shown in Figure 7(c), we see that the decomposition capacity with an in-

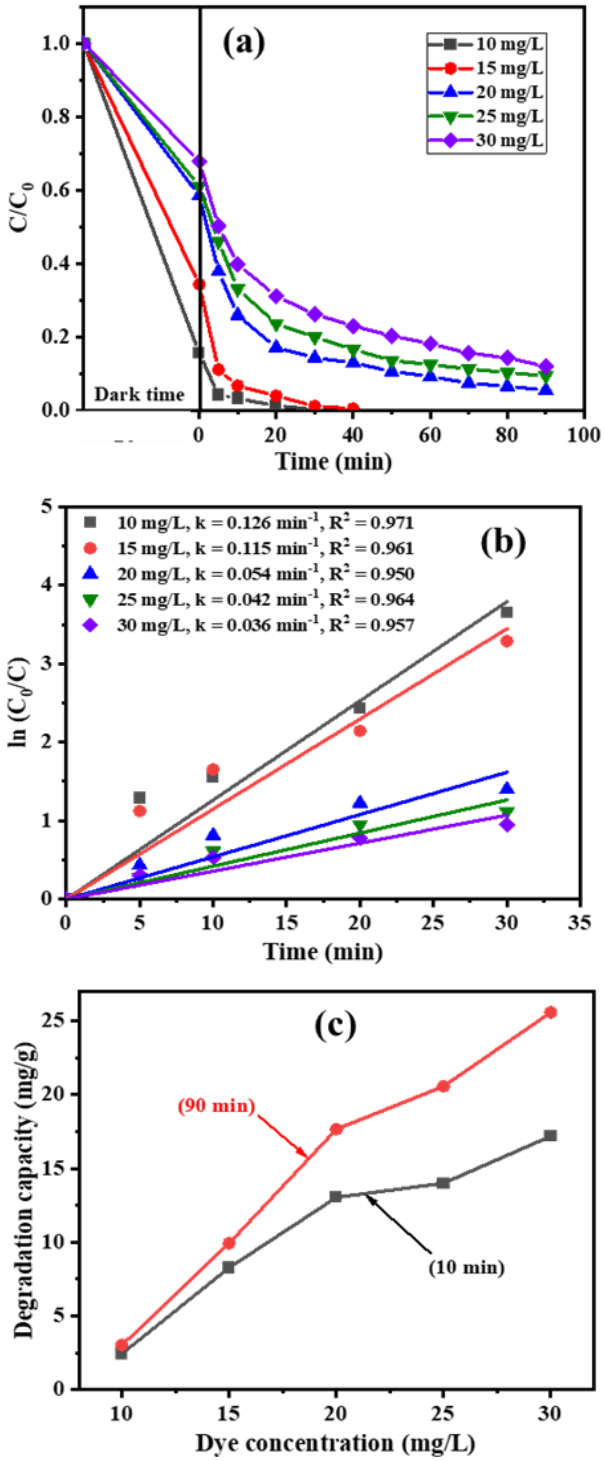

Figure 7. (a) Effect of initial TCH concentration on photocatalytic efficiency of B/ZnO materials; (b) Kinetic curves and (c) Degradation capacity.

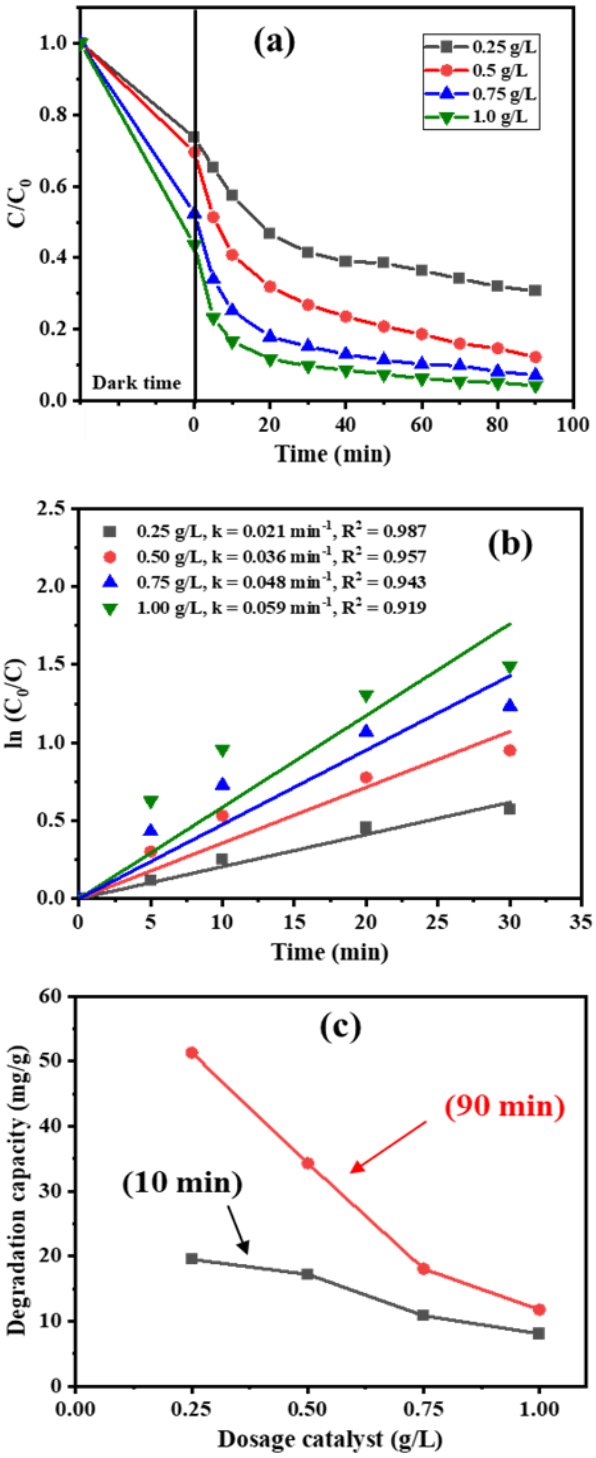

Figure 8. (a) Effect of B/ZnO catalyst concentration on TCH degradation efficiency; (b) Kinetic curves and (c) Degradation capacity.

itial TCH concentration of 30 mg/L in 10 and 30 min were 17.19 and 25.58 mg/g, respectively, which were higher than other concentrations.

3.3.2 Catalyst content

Figure 8 shows the effect of catalyst mass on the degradation of TCH. When the catalyst content used increased from 0.25 g/L to 1.00 g/L, the TCH decomposition efficiency also increased under the same reaction conditions as the initial concentration of TCH solution of 30 mg/L and the light source of a 250 W Hg lamp. Looking at Figure 8(a), we see that, in 90 min, when the catalyst content was 0.25 g/L, the TCH degradation efficiency was 58%. At the catalyst content of 1.00 g/L, about 90% TCH was decomposed. The value of the rate constant *k,* corresponding to the B/ZnO content of 0.25, 0.50, 0.75, and 1.00 g/L, were 0.021, 0.036, 0.048, and 0.059 min^{-1}, respectively. However, as shown in Figure 8(c), the decomposition capacity of TCH per gram of catalyst for 10 and 90 min were decreased with increasing catalyst content. The influence of catalyst mass on the degradation process could be explained by the following reasons: an increase in catalyst mass leads to an increase in the number of active sites available on the catalyst surface and the density of the catalyst particles in the illuminated area. Therefore, the photocatalytic ability of the material is leading to a rapid increase in antibiotic degradation efficiency [28,29]. However, because the catalyst mass increased faster than the degradation efficiency, the antibiotic degradation capacity was decreased while the reaction efficiency and rate could be improved.

3.3.3 The pH of the initial antibiotic solution

The pH value of the starting solution is also an important parameter in the photocatalysis of the material [30]. In this study, the effect of initial solution pH on TCH depletion was investigated in the pH range from 2 to 11. under fixed conditions (catalyst content 0.5 g/L, initial TCH concentration 20 mg/L, and the light source of 250 W Hg lamp), and the results are shown in Figure 10.

The TCH structure consists of rings connected with many ionizable functional groups. TCH could exist in different forms because of the three pKa. With a pH below 3.3, TCH was converted to the cation TCH^{3+} by protonating the dimethyl-ammonium group. In the pH range = 3.3–7.3, TCH existed as an amphoteric ion (TCH^0) due to the loss of a proton from the phenolic diketone radical. At the pH higher than 7.3, TCH converted to anionic form (TCH^- and TC^{2-}) due to proton loss from the tricarbonyl group and phenolic diketone radical [31]. In addition, the UV-Vis spectrum of TCH at different pH also showed a correlation between the pH values and a change in the absorption spectrum of the antibiotic (Figure 9).

For solutions with pH of 2, 4, 6, 9 and 11, the first order rate constants of antibiotic degradation were 0.001, 0.055, 0.050, 0.048, and 0.045 min^{-1}, respectively (Figure 10(b)). It was found that in the pH range from 4 to 11, the rate constant of TCH decomposition was almost the same and the optimal pH for efficient degradation of TCH on B/ZnO material was 4. In 90 min, 97% of TCH had been decomposed. Degradation capacities of TCH at 10 and 30 min were 13.59 and 24.12 mg/g, respectively, (Figure 10(c)). At pH = 2, the TCH degradation efficiency was almost non-existent, which was because of that ZnO was dissolved in an acidic

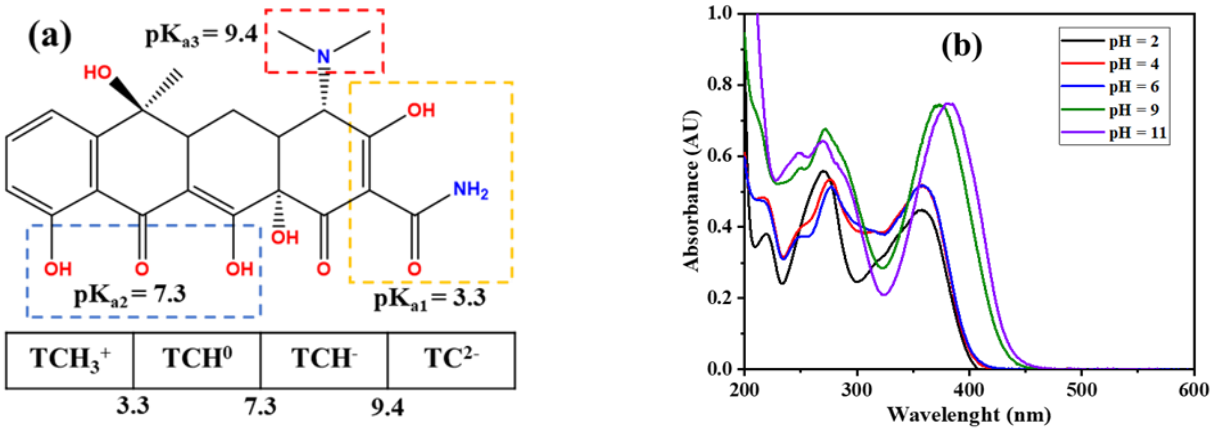

Figure 9. (a) Structure and pH-dependent surface speciation of TCH, (b) The UV-vis absorption spectra of TCH at different pH.

environment to give the corresponding salt ($ZnO_{(s)} + 2H^+_{(aq)} \rightarrow Zn^{2+} + H_2O$).

In addition, the surface charge properties of the nanoparticles are also pH dependent. The pH_{PZC} value of a material is the pH value at which the surface charge is zero. When the pH is below the pH_{PZC} value, the solution gives more H^+ ions than OH^- ions, so the catalyst surface becomes positively charged, resulting in better anion adsorption. Similarly, when the pH is higher than the pH_{PZC} value, the adsorbent surface carries a negative charge, which will better adsorb cations [12,32]. The pH_{PZC} value of B/ZnO was studied to reach 7.6 as shown in Figure 10(d). Therefore, at pH = 11, the catalyst surface poorly adsorbs TCH anions and lead to a significant decrease in antibiotic degradation with a reaction rate of 0.045 min^{-1}. But the highest TCH degradation capacities at 10 and 30 min were 17.07 and 31.72 mg/g, respectively. Which significantly increased compared to other pHs (Figure 10c). This can be explained that: at pH = 11, solution creates the large amount of OH^- ions on the surface of the nanoparticles as well as in the reaction medium, facilitating the formation of •OH. As a result, the degradation capacity increased but the efficiency and reaction rate were decreased.

3.4 Recovery and Reuse of B/ZnO Materials

One of the important factors determining the economic efficiency of materials in industrial applications is the reusability of the catalyst. In this study, the reusability of B/ZnO materials was evaluated through the photocatalytic efficiency of TCH on catalyst after three consecutive cycles. After first treatment, the powder catalyst was filtered, washed with distilled water and ethanol several times, dried at 80 ℃ for 12 h, and then reused for the next experiment. As the results showed in Figure 11, the efficiency of TCH degradation by B/ZnO under a 250 W Hg lamp was decreased from 90% to 46% after three consecutive cycles. This showed that B/ZnO was a less stable material with limited recovery and reuse. Therefore, improvements are needed to overcome this limita-

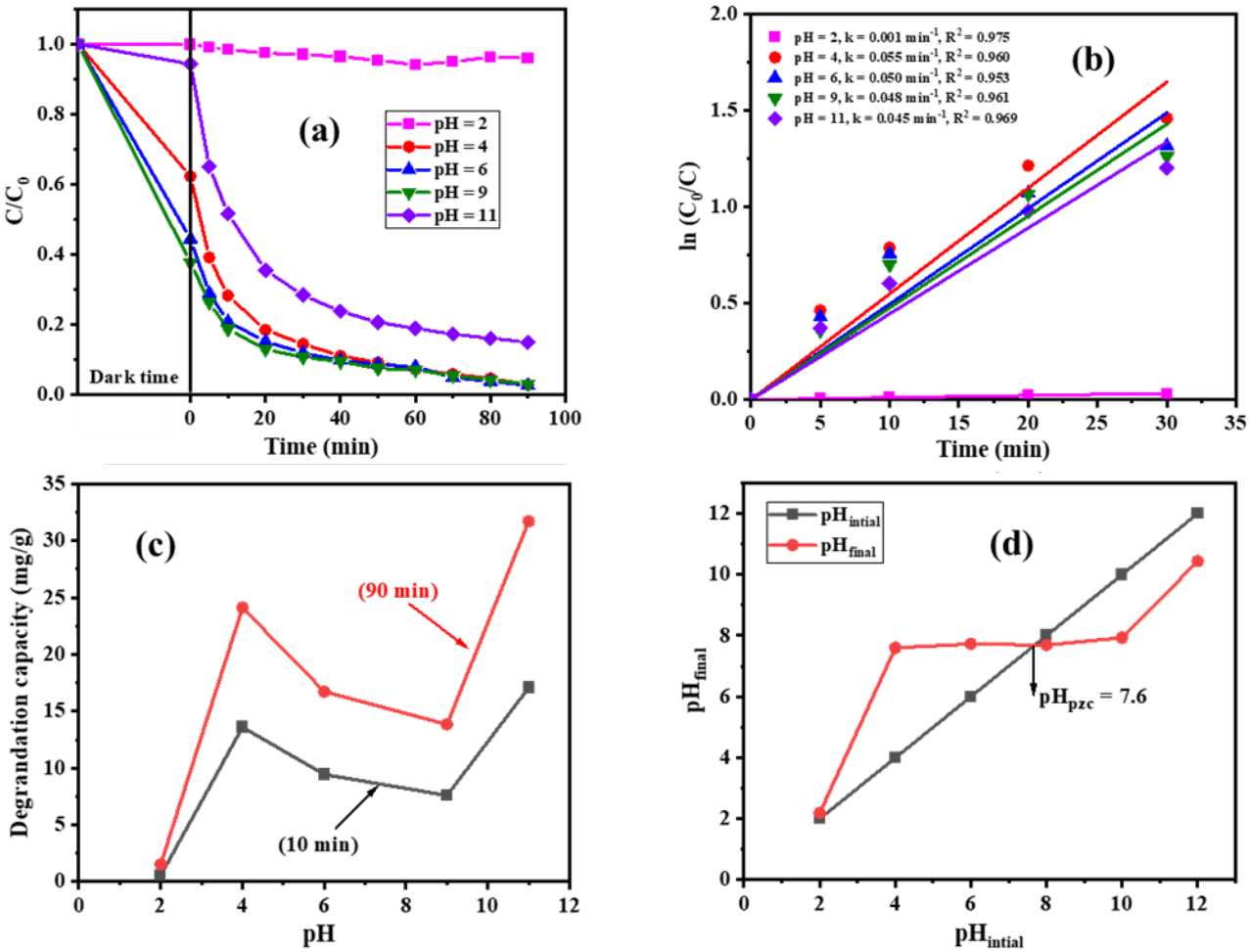

Figure 10. (a) Effect of pH of the initial TCH solution on the photocatalytic efficiency of B/ZnO; (b) Kinetic curves; (c) TCH degradation capacity at different pH and (d) pHPZC determination graph.

tion so that the material can be put into practical applications in wastewater treatment. The decrease in TCH degradation efficiency can be attributed to the loss of active sites after regeneration, the reduction of the interaction surface, and the partial dissolution of the catalyst after each experiment.

3.5 Photocatalyst Mechanism

The photocatalytic mechanism of B/ZnO material is shown in Figure 12. When there is an incident photon energy higher than the band gap energy of B/ZnO, the electron in the valence band (VB) is excited and jumps to the conduction band (CB) with a higher energy level, and at the same time in the region valence appears holes. The electron-hole pairs (e^- and h^+) and charge, can interact with oxygen and water on the surface of B/ZnO materials to produce oxidizing substances including H_2O_2, $\cdot O_2^-$, and other substances. original $\cdot$OH. Under the effect of the light of the Hg lamp, the $\cdot O_2^-$ and OH agents will combine with antibiotic molecules to form intermediate compounds by oxidation, mineralization, etc., and finally convert into harmless compounds CO_2 and H_2O.

We have the following reaction scheme:

$$H_2O \rightarrow H^+ + OH^- \quad (6)$$

$$ZnO + h\nu \rightarrow ZnO\ (e^- + h^+) \quad (7)$$

$$e^- + O_2 \rightarrow \cdot O_2^- \quad (8)$$

$$\cdot O_2^- + H^+ \rightarrow HO_2\cdot \quad (9)$$

$$HO_2\cdot + HO_2\cdot \rightarrow H_2O_2 + O_2 \quad (10)$$

$$H_2O_2 + h\nu \rightarrow 2\cdot OH \quad (11)$$

$$h^+ + OH^- \rightarrow \cdot OH \quad (12)$$

Because boron is an electron-deficient substance, it is easy to attract OH^- to the surface of the material, increasing the ability to create $\cdot$OH oxidizing radicals, thereby improving the photocatalytic performance of ZnO. Boron can act as an electron trap that prolongs the lifetime of electrons and holes [33]. The band gap energy of ZnO decreases when it is further doped with boron, thus B/ZnO materials easily absorb light energy to create electron-hole pairs (h^+ and e^-). Therefore, B/ZnO materials have a higher photocatalytic performance of TCH decomposition than ZnO.

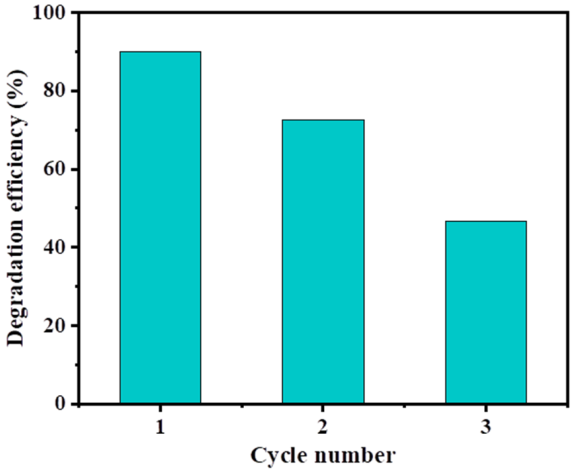

Figure 11. The regeneration capacity of B/ZnO after three consecutive TCH degradation cycles.

4. Conclusion

Successfully synthesized ZnO and B/ZnO materials by simple mechanical combustion method. The ZnO sample with irregular morphology and unequal size was formed from ZnO nanoparticles with the size of about 30–80 nm, they were tightly arranged together. B doping did not change the original structure of zinc oxide. The structure of B/ZnO became tighter and formed aggregation forms. Furthermore, the ZnO particle size was decreased to about 30–50 nm. The optimal content of doped B on ZnO was 3 wt%. The study of factors affecting the photocatalytic ability to degrade TCH of B/ZnO materials showed that the optimal conditions were: initial concentration of TCH solution was 10 mg/L, the appropriate catalyst content was 0.5 g/L, and the initial solution pH was 4.

Acknowledgments

The authors are grateful for the financial support Vietnam National Foundation for Science and Technology Development (NAFOSTED) under grant number 104.05-2018.333.

CRediT Author Statement

Author Contributions: Thu Huong Nguyen: Methodology, Investigation, Resources, Experiment and Writing; Anh-Tuan Vu: Review, Editing, and Validation. All authors have read and agreed to the published version of the manuscript.

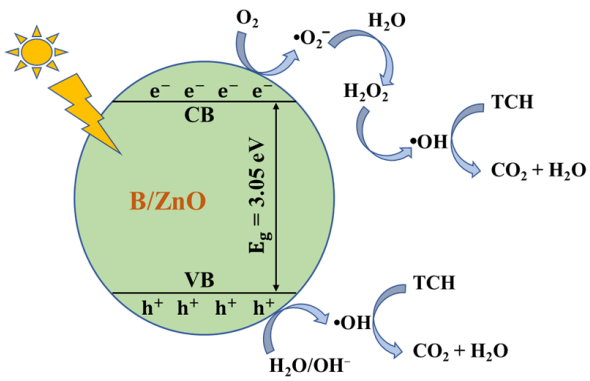

Figure 12. Photocatalytic mechanism of B/ZnO materials.

References

[1] Hao, R., Xiao, X., Zuo, X., Nan, J., Zhang, W. (2012). Efficient adsorption and visible-light photocatalytic degradation of tetracycline hydrochloride using mesoporous BiOI microspheres. *Journal of Hazardous Materials,* 209-210, 137-145. DOI: 10.1016/j.jhazmat.2012.01.006.

[2] Hoa, P.T.P., Managaki, S., Nakada, N., Takada, H., Shimizu, A., Anh, D.H., Viet, P.H., Suzuki, S. (2011). Antibiotic contamination and occurrence of antibiotic-resistant bacteria in aquatic environments of northern Vietnam. *Science of The Total Environment,* 409(15), 2894-2901. DOI: 10.1016/j.scitotenv.2011.04.030.

[3] Rizzo, L., Lofrano, G., Gago, C., Bredneva, T., Iannece, P., Pazos, M., Krasnogorskaya, N., Carotenuto, M. (2018). Antibiotic contaminated water treated by photo driven advanced oxidation processes: Ultraviolet/H_2O_2 vs ultraviolet/peracetic acid. *Journal of Cleaner Production,* 205, 67-75. DOI: 10.1016/j.jclepro.2018.09.101.

[4] Shejale, K.P., Yadav, D., Patil, H., Saxena, S., Shukla, S. (2020). Evaluation of techniques for the remediation of antibiotic-contaminated water using activated carbon. *Molecular Systems Design & Engineering,* 5(4), 743-756. DOI: 10.1039/c9me00167k.

[5] Pei, C.-Y., Chen, Y.-G., Wang, L., Chen, W., Huang, G.-B. (2021). Step-scheme WO3/CdIn2S4 hybrid system with high visible light activity for tetracycline hydrochloride photodegradation. *Applied Surface Science,* 535, 147682. DOI: 10.1016/j.apsusc.2020.147682.

[6] Pawinrat, P., Mekasuwandumrong, O., Panpranot, J. (2009). Synthesis of Au–ZnO and Pt–ZnO nanocomposites by one-step flame spray pyrolysis and its application for photocatalytic degradation of dyes. *Catalysis Communications,* 10(10), 1380-1385. DOI: 10.1016/j.catcom.2009.03.002.

[7] Pereira, J.H.O.S., Vilar, V.J.P., Borges, M.T., González, O., Esplugas, S., Boaventura, R.A.R. (2011). Photocatalytic degradation of oxytetracycline using TiO_2 under natural and simulated solar radiation. *Solar Energy,* 85(11), 2732-2740. DOI: 10.1016/j.solener.2011.08.012.

[8] Viet, N.M., Trung, D.Q., Giang, B.L., Tri, N.L.M., Thao, P., Pham, T.H., Kamand, F.Z., Al Tahtamouni, T.M. (2019). Noble metal - doped graphitic carbon nitride photocatalyst for enhancement photocatalytic decomposition of antibiotic pollutant in wastewater under visible light. *Journal of Water Process Engineering,* 32, 100954. DOI: 10.1016/j.jwpe.2019.100954.

[9] Thi, T.A.N., Vu, A.T. (2022). Nanocomposite ZnO/g-C3N4 for Improved Degradation of Dyes under Visible Light: Facile Preparation, Characterization, and Performance Investigations. *Bulletin of Chemical Reaction Engineering & Catalysis,* 17(2), 403-419. DOI: 10.9767/bcrec.17.2.13931.403-419.

[10] Andrade, G.R.S., Nascimento, C.C., Silva Júnior, E.C., Mendes, D.T.S.L., Gimenez, I.F. (2017). ZnO/Au nanocatalysts for enhanced decolorization of an azo dye under solar, UV-A and dark conditions. *Journal of Alloys and Compounds,* 710, 557-566. DOI: 10.1016/j.jallcom.2017.03.295.

[11] Cheng, Y.E., Jiao, W., Li, Q., Zhang, Y., Li, S., Li, D., Che, R. (2018). Two hybrid Au-ZnO aggregates with different hierarchical structures: A comparable study in photocatalysis. *Journal of Colloid and Interface Science,* 509, 58-67. DOI: 10.1016/j.jcis.2017.08.077.

[12] Verma, S., Rao, B.T., Jayabalan, J., Rai, S.K., Phase, D.M., Srivastava, A.K., Kaul, R. (2019). Studies on growth of Au cube-ZnO core-shell nanoparticles for photocatalytic degradation of methylene blue and methyl orange dyes in aqueous media and in presence of different scavengers. *Journal of Environmental Chemical Engineering,* 7(4), 103209. DOI: 10.1016/j.jece.2019.103209.

[13] Tuan, V.A., Tuyet, P.T.A., Truong, D.X., Anh, T.V., Duong, L.V., Duc, T.D., Huu, N.T., Viet, N.M. (2021). Preparation of Hierarchical Structure Au/ZnO Composite for Enhanced Photocatalytic Performance: Characterization, Effects of Reaction Parameters, and Oxidizing Agent Investigations. *Adsorption Science & Technology*, 2021, 5201497. DOI: 10.1155/2021/5201497.

[14] Wu, J.-J., Tseng, C.-H. (2006). Photocatalytic properties of nc-Au/ZnO nanorod composites. *Applied Catalysis B: Environmental,* 66(1-2), 51-57. DOI: 10.1016/j.apcatb.2006.02.013.

[15] Tuyet, P.T.A., Anh, T.V., Duong, L.V., Viet, N.M., Duc, T.D., Truong, D.X., Anh, T.V. (2020). Facile preparation of ZnO nanoparticles and Ag/ZnO nanocomposite and their photocatalytic activities under visible light. *International Journal of Photoenergy*, 2020, 8897667. DOI: 10.1155/2020/8897667.

[16] Ren, C., Yang, B., Wu, M., Xu, J., Fu, Z., Iv, Y., Guo, T., Zhao, Y., Zhu, C. (2010). Synthesis of Ag/ZnO nanorods array with enhanced photocatalytic performance. *Journal of Hazardous Materials,* 182(1-3), 123-9. DOI: 10.1016/j.jhazmat.2010.05.141.

[17] Tuan, V.A., Tuyet, P.T.A., Thuy, T.T., Truong, N.X., Quynh, T.T., Tung, T.Q., Nghia, N.T., Van, D.T., Duong, V.T., Long, N.C., Viet, N.M., Ha, L.C. (2020). Synthesis of Nano-Flakes Ag•ZnO•Activated Carbon Composite from Rice Husk as A Photocatalyst under Solar Light. *Bulletin of Chemical Reaction Engineering & Catalysis,* 15(1), 264-279. DOI: 10.9767/bcrec.15.1.5892.264-279.

[18] Ahmed, A.Z., Islam, M.M., Islam, M.M.u., Masum, S.M., Islam, R., Molla, M.A.I. (2020). Fabrication and characterization of B/Sn-doped ZnO nanoparticles via mechanochemical method for photocatalytic degradation of rhodamine B. *Inorganic and Nano-Metal Chemistry*, 51(10), 1369–1378. DOI: 10.1080/24701556.2020.1835976.

[19] Liu, Z., Cai, X., Fan, S., Zhang, Y., Hu, H., Huang, Z., Liang, J., Qin, Y. (2021). Preparation of a stable polyurethane sponge supported Sn-doped ZnO composite via double-template-regulated bionic mineralization for visible-light-driven photocatalytic degradation of tetracycline. *Journal of Environmental Chemical Engineering,* 9(4), 105541. DOI: 10.1016/j.jece.2021.105541.

[20] Núñez-Salas, R.E., Rodríguez-Chueca, J., Hernández-Ramírez, A., Rodríguez, E., Maya-Treviño, M.d.L. (2021). Evaluation of B-ZnO on photocatalytic inactivation of Escherichia coli and Enterococcus sp. *Journal of Environmental Chemical Engineering,* 9(1), 104940. DOI: 10.1016/j.jece.2020.104940.

[21] Kabir, R., Saifullah, M.A.K., Ahmed, A.Z., Masum, S.M., Molla, M.A.I. (2020). Synthesis of N-Doped ZnO Nanocomposites for Sunlight Photocatalytic Degradation of Textile Dye Pollutants. *Journal of Composites Science,* 4(2), 49. DOI: 10.3390/jcs4020049.

[22] Patil, A.B., Patil, K.R., Pardeshi, S.K. (2011). Enhancement of oxygen vacancies and solar photocatalytic activity of zinc oxide by incorporation of nonmetal. *Journal of Solid State Chemistry,* 184(12), 3273-3279. DOI: 10.1016/j.jssc.2011.10.016.

[23] Wang, W., Ai, T., Yu, Q. (2017). Electrical and photocatalytic properties of boron-doped ZnO nanostructure grown on PET-ITO flexible substrates by hydrothermal method. *Scientific Reports*, 7, 42615. DOI: 10.1038/srep42615.

[24] Yi, S., Cui, J., Li, S., Zhang, L., Wang, D., Lin, Y. (2014). Enhanced visible-light photocatalytic activity of Fe/ZnO for rhodamine B degradation and its photogenerated charge transfer properties. *Applied Surface Science,* 319, 230-236. DOI: 10.1016/j.apsusc.2014.06.151.

[25] Yu, Q., Li, J., Li, H., Wang, Q., Cheng, S., Li, L. (2012). Fabrication, structure, and photocatalytic activities of boron-doped ZnO nanorods hydrothermally grown on CVD diamond film. *Chemical Physics Letters,* 539-540, 74-78. DOI: 10.1016/j.cplett.2012.04.051.

[26] Ngoc, K.H.P., Vu, A.T. (2022). Simple Preparation of the CuO• Fe3O4/Silica Composite from Rice Husk for Enhancing Fenton-Like Catalytic Degradation of Tartrazine in a Wide pH Range. *Adsorption Science & Technology*, 2022, 6454354. DOI: 10.1155/2022/6454354.

[27] Tu, V.A., Tuan, V.,A. (2018). A facile and fast solution chemistry synthesis of porous ZnO nanoparticles for high efficiency photodegradation of tartrazine. *Vietnam Journal of Chemistry,* 56(2), 214-219. DOI: 10.1002/vjch.201800016.

[28] Mai, L.T., Hoai, L.T., Tuan, V.A. (2018). Effects of reaction parameters on photodegradation of caffeine over hierarchical flower-like ZnO nanostructure. *Vietnam Journal of Chemistry,* 56(5), 647-653. DOI: 10.1002/vjch.201800064.

[29] Behnajady, M.A., Modirshahla, N., Hamzavi, R. (2006). Kinetic study on photocatalytic degradation of C.I. Acid Yellow 23 by ZnO photocatalyst. *Journal of Hazardous Materials,* 133(1-3), 226-232. DOI: 10.1016/j.jhazmat.2005.10.022.

[30] Krishnakumar, B., Selvam, K., Velmurugan, R., Swaminathan, M. (2012). Influence of operational parameters on photodegradation of Acid Black 1 with ZnO. *Desalination and Water Treatment,* 24(1-3), 132-139. DOI: 10.5004/dwt.2010.1466.

[31] Liu, M., Hou, L.A., Yu, S., Xi, B., Zhao, Y., Xia, X. (2013). MCM-41 impregnated with A zeolite precursor: Synthesis, characterization and tetracycline antibiotics removal from aqueous solution. *Chemical Engineering Journal,* 223(100), 678-687. DOI: 10.1016/j.cej.2013.02.088.

[32] Bechambi, O., Najjar, W., Sayadi, S. (2016). The nonylphenol degradation under UV irradiation in the presence of Ag–ZnO nanorods: Effect of parameters and degradation pathway. *Journal of the Taiwan Institute of Chemical Engineers,* 60, 496-501. DOI: 10.1016/j.jtice.2015.11.017.

[33] Núñez-Salas, R.E., Hernández-Ramírez, A., Hinojosa-Reyes, L., Guzmán-Mar, J.L., Villanueva-Rodriguez, M., de Lourdes Maya-Trevino, M.J.C.T. (2019). Cyanide degradation in aqueous solution by heterogeneous photocatalysis using boron-doped zinc oxide. *Catalysis Today*, 328, 202-209. DOI: 10.1016/j.cattod.2018.11.061.